Journal of Molecular Graphics and Modelling 30 (2011) 179–185

Contents lists available at ScienceDirect

Journal of Molecular Graphics and Modelling

journal homepage: www.elsevier.com/locate/JMGM

Atomic-scale characterization of conformational changes in the preQ$_1$ riboswitch aptamer upon ligand binding

Paula M. Petrone, Janetta Dewhurst, Ruben Tommasi, Lewis Whitehead*, Andrea K. Pomerantz**

Novartis Institutes for BioMedical Research, Inc., 100 Technology Square & 250 Massachusetts Ave. Cambridge, MA 02139, United States

ARTICLE INFO

Article history:
Received 16 June 2011
Received in revised form 14 July 2011
Accepted 14 July 2011
Available online 22 July 2011

Keywords:
preQ$_1$ riboswitch
Molecular dynamics
Fluorescence spectroscopy
Pre-queosine
mRNA

ABSTRACT

Riboswitches are mRNA structural elements that act as intracellular sensors of small-molecule metabolites. By undergoing conformational changes capable of modulating translation or terminating transcription, riboswitches are able to play a role in regulating the concentration of essential metabolites in the cell. Computer-guided fluorescence experiments were carried out to interrogate molecular dynamics and conformational changes in the minimal riboswitch aptamer that binds 7-aminomethyl-7-deazaguanine (preQ$_1$). Our combined experimental results and computational analysis suggest that the preQ$_1$ riboswitch apo form is structured but shows no evidence of a ligand-binding pocket. Simulations of the apo and bound forms indicate a large conformational change is triggered by the breaking of the Watson–Crick base pairing of nucleotides G11 and C31 upon preQ$_1$ removal, followed by collapse of the pocket due to interfering π-stacking. Computational predictions of local aptamer dynamics were validated by fluorescence experiments employing 2-aminopurine substitutions. In-line probing reactions confirmed that fluorophore-labeled riboswitches retain similar higher-order structural features as the unlabeled aptamer upon ligand binding, although their affinity for the ligand is reduced by the introduction of the fluorescent reporter.

1. Introduction

Riboswitches are genetic regulatory elements of mRNA capable of adopting two mutually exclusive conformations triggered by an environmental signal such as temperature change or the binding of a small molecule; to date, they have been found in bacteria, plants, fungi, and archaea [1]. Usually, a riboswitch sequence is found in the 5′ untranslated region preceding genes required for the biosynthesis of its cognate ligand. Conformational changes in the riboswitch promote interaction with downstream mRNA and protein components involved in gene expression, eliciting either premature transcription termination or inhibition of translation, which is subsequently propagated down the metabolic pathway. The study of riboswitch dynamics has been approached both experimentally [1] and *in silico* by bioinformatics [2] and molecular dynamics (MD) simulations [3–5].

A lack of X-ray crystal structures of riboswitches in the unbound form leaves numerous unresolved questions regarding riboswitch folding and binding at the atomic level. Multiple research groups have investigated the nature of the apo state of certain riboswitch aptamers, and the results and conclusions they draw do not appear to follow a general pattern. For example, work done by Batey and collaborators [5] depicts the ligand-free state of the *S*-adenosylmethionine (SAM-I) riboswitch not as a single conformation but rather as an ensemble of states that minimizes the energy barrier between the free and bound states. Meanwhile, for the same SAM-responsive riboswitch, Wilson et al. have characterized distinct, mutually exclusive RNA conformations in the presence or in the absence of the effector metabolite using NMR [7]. In contrast, crystallography studies of the lysine riboswitch show almost identical apo and liganded structures [8,9]. Similarly, NMR results [10] support the existence of a partially organized binding pocket in the apo guanine/adenine riboswitch aptamer, a finding which is also supported by MD simulations [3,4,11]. In the case of the preQ$_1$ aptamer, the NMR work of Feigon et al. [12,13] has provided evidence as to which regions are more flexible than others in the ligand-bound structure; moreover, their study points to interactions that seem to differ between the bound and free preQ1 aptamer. The nature of the unbound state, the dynamic behavior of the ligand-binding pocket, and the role that counter ions play are questions that we address here by deriving a structural model and validating our predictions with 2-aminopurine-based fluorescence measurements of riboswitch conformational change.

The preQ$_1$ Class I riboswitch of *Bacillus subtilis* was used as a model system for this investigation because its aptamer has an unusually short sequence (34 nucleotides) but retains all of the

* Corresponding author. Tel.: +1 617 871 7115.
** Corresponding author. Tel.: +1 617 871 5289.
E-mail addresses: lewis.whitehead@novartis.com (L. Whitehead), andrea.pomerantz@novartis.com (A.K. Pomerantz).

1093-3263/$ – see front matter © 2011 Elsevier Inc. All rights reserved.
doi:10.1016/j.jmgm.2011.07.006

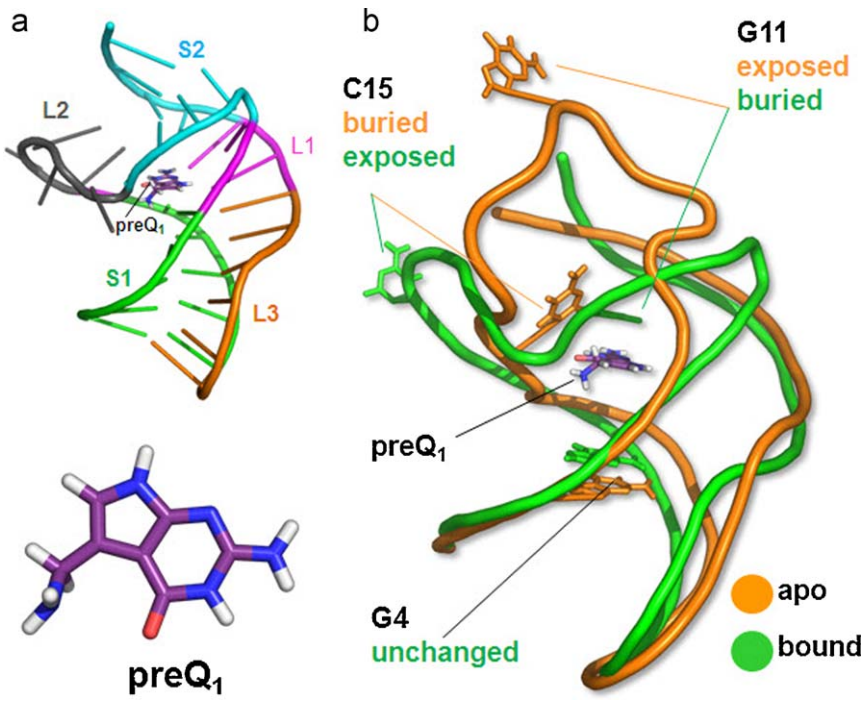

Fig. 1. (a) Structural features of $preQ_1$ riboswitch are defined as in the crystal structure [17] and following the same color code (top); structure of ligand preQ1 (bottom). (b) Bound (green) crystal structure and prediction of apo (orange) from MD simulations. Shown in sticks, key nucleotides G4, G11, and C15 are predicted to become unchanged, buried, and exposed, respectively, upon $preQ_1$ ligand binding.

features of larger riboswitch aptamers (conformational change, nanomolar ligand binding affinity and selectivity, and conserved pseudoknot motif) [14]. Riboswitch $preQ_1$ binds 7-aminomethyl-7-deazaguanine ($preQ_1$), a precursor metabolite in the biosynthetic pathway of queuosine [15,16], which is a hypermodified nucleoside implicated in bacterial virulence [15] and translational fidelity [16]. The *B. subtilis* $preQ_1$ aptamer folds into an H-type pseudoknot [12,17], as illustrated in Fig. 1(a). Loops L1 and L3 lie in the grooves of stem S2 and S1 respectively, while nucleotides in L3 form triplex interactions with Watson–Crick pairs in S2. The ligand $preQ_1$ is intercalated at the helical interface between two Watson–Crick pairs (G11–C31 and G5–C18). C17 forms a Watson–Crick pair with $preQ_1$, which is 92% buried. C15 is reported to be extruded into solvent [17], and nucleotides C12 and U13 of the L2 loop are disordered in the wild-type X-ray structure.

The $preQ_1$ riboswitch has been characterized using biophysical [18,19], X-ray crystallographic [17,20], and NMR [12,13,18,19] methods, and more recently using $G^{\bar{o}}$-model simulations [21]. Roth et al. showed that the $preQ_1$ riboswitch regulates transcription in vitro [14], while Klein [17], Kang [12] and coworkers proposed that the pseudoknotted fold of the aptamer domain competed with the formation of the transcriptional terminator. In another recent study, Micura et al. used 2-aminopurine (2-AP) fluorescence measurements to provide evidence for the formation of two competing stem-loop structures in the expression platform of the full-length $preQ_1$ riboswitch domain; the relative populations of these structures were shifted upon formation of the ligand-binding complex [19]. Sporadic sequence conservation in the $preQ_1$ riboswitch family does not guarantee the universality of this mechanism, but Micura and coworkers established the bistable character of the full $preQ_1$ riboswitch, i.e., its capability of adopting two different and coexisting conformations. Brooks et al. [21] published a study of the folding pathway of the $preQ_1$ riboswitch using Go models. In that study, the authors used a potential that is topologically biased towards the bound state in order to explore the folding pathway of the aptamer. As might be expected, they report that in the presence of the ligand, they do not find any rate-limiting intermediate states that could pose significant barriers along the folding reaction coordinate. Because their simulation is driven by interactions that only occur in the bound state, their study focuses on aptamer folding in the presence of the effector ligand, whereas our work focuses on elucidating changes that occur in both the presence and in the absence of the ligand, and for that we employ transferable MD force field potentials that are independent of the system of study. Our work is centered around the behavior of the aptamer region of the $preQ_1$ riboswitch, in particular to elucidate the nature of the apo form and to explore ligand-driven changes in the aptamer domain itself. Using all-atom MD simulations, starting from the aptamer liganded state, we predict the apo state without introducing topological biases. By analyzing the solvent-accessible surface per nucleotide, as well as structural fluctuations and interaction maps from the MD simulation for both the bound and unbound states, we make a hypothesis of the structural rearrangements that result from ligand binding. Combining these analyses, we identify both invariant as well as flexible regions that undergo conformational change upon ligand unbinding, and we select a subset of representative nucleotides for fluorescence reporter measurements. With a set of 2-AP-substituted riboswitch constructs, we monitor fluorescence to obtain readout of ligand-induced local structural changes in the regions identified from our computational predictions. We then compare the data about the end-states from both in vitro and *in-silico* experiments in order to formulate a model for key atomic-scale steps in $preQ_1$ ligand recognition and riboswitch aptamer dynamics.

2. Materials and methods

2.1. Experimental methods

2.1.1. Synthesis of $preQ_1$

Synthesis of $preQ_1$ was carried out based on the protocols in Refs. [14,22]; further details are included in Supplementary data.

2.1.2. RNA constructs

All four RNA sequences used in these experiments are derived from the 34-nucleotide (nt) preQ$_1$ riboswitch aptamer from *B. subtilis*. PQ1c consists of unmodified RNA, while constructs 2AP4, 2AP11 and 2AP15 bear a single 2-aminopurine (2-AP) substitution at nucleotide G4, G11 and C15, respectively, of the 34 nt aptamer sequence. Synthetic RNA oligonucleotides were purchased from Thermo Scientific Dharmacon. All sequences were deprotected and desalted before use.

2.1.3. Fluorescence spectroscopy

Steady-state fluorescence measurements were carried out following the method described by Micura et al. [19]. 2-AP-labeled riboswitch constructs were prepared at 1 μM concentration in a total volume of 1 mL of 1× riboswitch buffer (50 mM Tris–HCl, 20 mM $MgCl_2$, 100 mM KCl, pH 8.3). 2 mM preQ$_1$ stock solution was prepared by dissolving 0.4 mg of preQ$_1$ (MW 239.23) in 836 μL 1× riboswitch buffer. 2 mM adenine stock solution was prepared for control samples by dissolving 0.5 mg of adenine (MW 135.1) in 1850 μL 1× riboswitch buffer. Both solutions were heated at 37 °C for 10 min to ensure thorough sample dissolution. Prior to metabolite addition, RNA samples were annealed by heating at 90 °C for 2 min, followed by incubation at room temperature over a period of 30 min prior to analysis. Samples were transfered to quartz cuvettes, and preQ$_1$ was manually pipetted in 1 μL aliquots so as not to exceed a total volume increase of 2%. The solution was allowed to equilibrate for at least 10 min before data collection. Spectra were recorded on a SpectraMax M5 multi-mode microplate reader (Molecular Devices) using the following measurement parameters: excitation wavelength, 308 nm; emission scan range, 320–500 nm; data acquisition interval, 2 nm. Data were fit to a K_D quadratic equation solution for 1:1 binding stoichiometry [19] using GraphPad Prism. Control samples with adenine or buffer-only additions to 2-AP-labeled riboswitch constructs were similarly prepared and analyzed; these displayed no significant change in 2-AP fluorescence emission.

2.1.4. In-line probing

Control in-line probing experiments were carried out using protocols adapted from Refs. [14,19,23]. Detailed protocols and data are provided in Supplementary data.

2.2. Computational methods

2.2.1. Modeling details

As a starting point for MD simulations, we used chain B of the X-ray crystal structure of preQ$_1$ riboswitch at 2.85 Å resolution (PDB ID: 3FU2) [17]. Missing nucleotides C12 and U13 were modeled in and energy-minimized using the NMR structure (PDB ID: 2KFC) [12] of riboswitch preQ$_1$ as a template. Initial coordinates for the preQ$_1$ ligand, crystallographic water and Ca^{2+} ions were retained, and excess negative charge was balanced by replacing 14 water molecules with 13 Mg^{2+} ions and 1 Na^+ ion. The final dimensions of the model are as follows: 29,329 atoms in a box of dimensions 78.5 Å × 62 Å × 60 Å, comprising the aptamer and 9164 molecules of TIP3P water [24], 2 Ca^{2+} ions, 1 Na^+ ion and 13 Mg^{2+} ions. AMBER charges for ligand preQ$_1$ were obtained using Jaguar, and their values are found in the range of Mulliken and RESP charges. The topology of the ligand preQ$_1$ was crafted by hand using guanine and tryptophan as templates for atom types and dihedrals. The initial Apo structure of preQ$_1$ aptamer was obtained by eliminating the preQ$_1$ ligand from the model of the bound structure and following identical simulation protocols (solvation and restrained equilibration).

2.2.2. Simulation details

We used the all-atom force field of AMBER 99-ϕ [25] modified by Sorin and Pande [26], as there is precedent in the literature for using this methodology in RNA MD simulations [5,6,27], thus allowing direct comparison of our results with previous work. A cutoff value of 14 Å was used for non-bonded electrostatic interactions. Long-range (>14 Å) electrostatic interactions were approximated with a reaction-field algorithm implemented in GROMACS 4 [28,29], with a dielectric constant of 78. All bonds were constrained using the LINCS algorithm [30]. We simulated each system using Berendsen temperature coupling [31] (constant N, V, T = 298 K ensemble (NVT)) for both equilibration and production. Simulation with pressure coupling (constant N, P = 1 atm, T = 298 K (NPT)) was used only for equilibration as detailed in the protocols below.

2.2.3. Equilibration protocol

Initially, the system was subject to energy minimization, followed by 200 ps of restrained NVT ensemble equilibration of the solvent with restrained riboswitch. Subsequently, 400 ps of unrestrained NVT equilibration was performed to achieve the target temperature of 298 K. Finally, 100 ps of NPT followed, in order to achieve the target density. The integration step was 0.002 ps. Configurations were saved for subsequent analysis at the rate of one snapshot per 10 ps. Production and total sampling lengths varied for different trajectories.

The total simulation times (excluding equilibration) were as follows: 570 ns for apo simulation, 470 ns for bound simulation. Only the final portion of the trajectories (350 ns (apo), 420 ns (bound)) was employed for data analysis of molecular properties. Details of the cluster analysis of the MD trajectory and RNA structure identification are provided in Supplementary data.

2.2.4. Calculation of solvent accessible surface area (SASA)

SASA was estimated using the program g_sasa implemented in the Gromacs 4 package [28,29] in its default settings (probe radius 0.14 nm).

3. Results and discussion

3.1. Computational prediction of preQ$_1$ aptamer dynamics

In the bound simulation, the ligand remained bound in the pocket for the entire simulation time, and the aptamer structure underwent no global conformational change (Movie 1). Conversely, in the ligand-free simulation, a conformational change was observed as the initial bound conformation was destabilized in the absence of the ligand. After the first 9 ns, a Mg^{2+} cation from the bulk solvent interacted with nucleobase G11. Furthermore, in the absence of π-stacking interactions with the preQ$_1$ ligand, Watson–Crick base pair G11–C31 was destabilized, and G11 flipped open, precipitating a large conformational change as illustrated in Fig. 1(b) and Movie 2.

Cations coordinated in the binding site of some riboswitches aid in ligand recognition and affinity, as reviewed in the work of Lipfert et al. [32]. In our simulation of the preQ$_1$ riboswitch aptamer, the crystallographic Ca^{2+} initially present in the pocket has a long residence time of 40 ns in the bound simulation and eventually migrates out of the pocket. In the apo simulation, Ca^{2+} was retained for 26 ns, even after collapse of the pocket. Recently, the work of Feigon et al. revealed that addition of Ca^{2+} to the aptamer-preQ$_1$ complex in solution produces conformational changes that could account for the differences between the solution and crystal structures. In our studies, we do not observe major conformational changes after the Ca^{2+} ion leaves the pocket. On the other hand, the fact that the ligand remains bound in our simulation in the absence

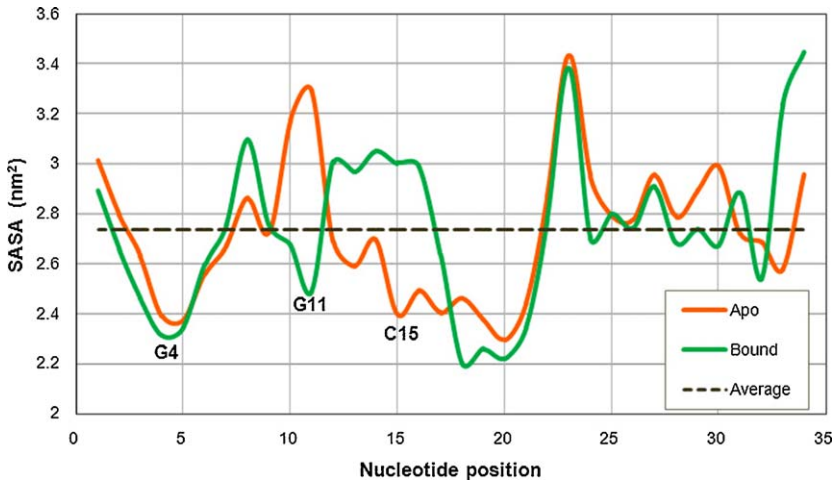

Fig. 2. Solvent accessible surface area (SASA) per nucleotide averaged over the production trajectory for both the apo and the bound simulation. The average SASA per nucleotide (2.74 nm^2) was calculated based on the bound simulation. For our analysis, nucleotides with SASA above average are referred to as "exposed" whereas nucleotides with below-average SASA are defined as "buried". In bold, nucleotides G4, G11 and C15 are highlighted. G11 and C15 undergo a large change of SASA between the bound and the unbound simulation. For G11, the percent change of SASA between bound and unbound is $(SASA_b - SASA_u)/SASA_b = -32\%$. For C15 the increase of SASA is approx. 20%.

of the coordinated Ca^{2+} ion is consistent with the observation by Feigon and coworkers that the Ca^{2+} ions present in the X-ray crystal structure, which were proposed to be important for folding and ligand recognition [17], are not required for either of these features in solution.

Fig. 2 shows the average solvent accessible surface area (SASA) per nucleotide for both the bound and the unbound simulation. SASA is a useful parameter that allows us to identify the regions that undergo a conformational transition between states of varying solvent exposure. For our analysis, nucleotides with SASA above average are referred to as "exposed" whereas nucleotides with below-average SASA are defined as "buried". Previous studies [33,34] indicate that 2-AP fluorescence tends to increase with solvent exposure and decrease with base stacking. We do not expect this relationship between 2-AP fluorescence and SASA to be linear given that 2-AP fluorescence also responds to changes in the local environment, including stacking of neighboring residues, but regional changes in SASA are compared to experimental measurements in the next section to aid in quantifying agreement between prediction and observation. Fig. 2 illustrates the general agreement between the SASA for the bound and the unbound states except for the region between nucleotides 10 and 18. The region between nucleotides 2 and 6 is invariant and buried, and nucleotide G4 arises as a candidate for 2-AP substitution to verify that this region does not change. Both G11 and C15 undergo a large change in SASA between the bound and the unbound simulation. For G11, the percent change in SASA between bound and unbound is $(SASA_b - SASA_u)/SASA_b = -32\%$; for C15, the SASA increase is approximately 20%.

Fig. 3 depicts the root mean square (RMS) fluctuations per nucleotide and provides insight into the flexibility of the different aptamer regions. While one would expect that binding of $preQ_1$ ligand would restrict RNA conformational fluctuations, it is noteworthy from the MD simulations that both apo and bound aptamer forms are very flexible. However, the regions of highest flexibility differ between apo and bound, with major differences found in the loop L2 segment, which is partially disordered in the X-ray crystal structure [17]. This observation from simulation agrees with previous reports [12,13] where the conformational flexibility of the riboswitch aptamer in the ligand-bound state was studied on pico- to nanosecond (ps–ns) timescales using NMR relaxation measurements. These NMR spin relaxation data revealed that L2 is the only highly dynamic region of the $preQ_1$-bound aptamer, consistent with loop L2 being disordered in the X-ray structure [12,13]. Likewise, minimal conformational change was reported in those studies for nucleotides 19, 20, and 32, all of which have very low RMS fluctuations in our simulation. C19 is Watson–Crick-paired with nucleotide G4, the latter of which we selected as a representative reporter for regions of minimal conformational change. As anticipated, regions found by both simulation and NMR methods to be flexible in the ligand-bound structure do correspond to regions of conformational diversity in a comparison of bound vs. our simulated apo conformations. Also notable in our simula-

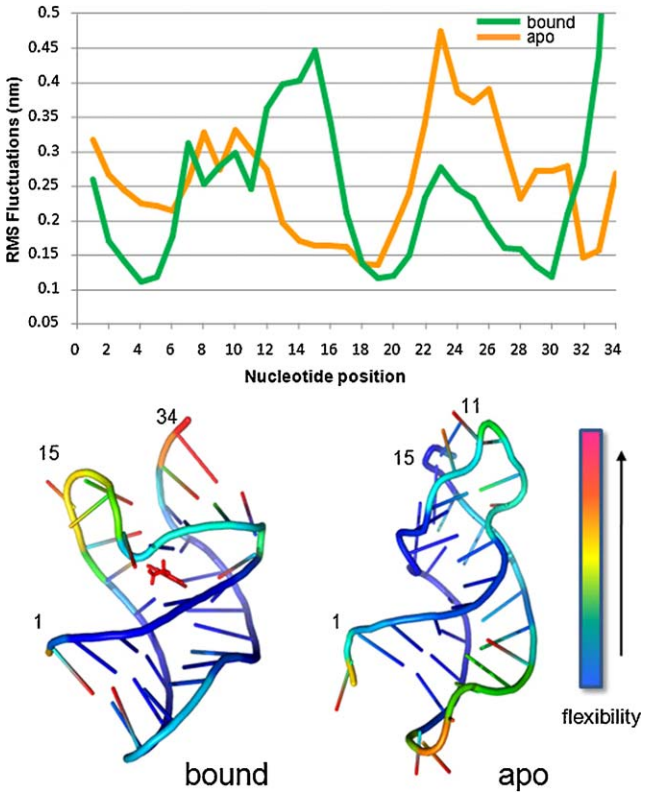

Fig. 3. Flexibility (root mean square fluctuations) of the bound and apo forms from MD simulations. Only the last portion of the trajectories was employed for data analysis of observables: 350 ns (apo), 420 ns (bound).

tion is the fact that loop L2 lacks flexibility in the unbound state due to tight π-stacking of its constituent nucleotides. The simulation timescales (ps–ns) are short compared to standard biological timescales (μs–ms), and so it is possible that the aptamer has been locked in a metastable state, or that we are observing only one conformation of the apo-state ensemble as discussed in the next section.

An unexpected feature regarding the RMSF of the bound state is that the 3′ end (nt 33–34) of the aptamer exhibits a high degree of conformational variability relative to the 5′ end, and relative to both ends in the apo state. Similar conformational variability is observed at the 3′ end of the NMR structure (Supplementary Fig. S14). It is possible that the nature of local interactions and the particular geometry of the 3′ end could contribute to the enhanced flexibility of this region, which might facilitate the formation of the two competing stem structures observed by Micura et al. [19]. However, it is plausible that this effect may be an artifact of employing a reduced riboswitch system where the aptamer is investigated in the absence of the expression platform.

The $preQ_1$ aptamer exhibits a rich diversity of base-pairing interactions that contribute to the complexity of the riboswitch tertiary structure. Along the MD trajectory, nucleotides flip, turn, and engage in different pairs and multiplets. Changes in base-pairing impact the RNA tertiary structure; we therefore employed a cluster method analysis to investigate these changes by characterizing the conformational variability of both the ligand-free and bound trajectories. A cluster analysis based on root mean square deviation (RMSD) was performed over all MD simulation snapshots. Cluster centers convey information about the predominant intra-riboswitch aptamer interactions and thus allow for identification of regions of major conformational change in the aptamer. The structural variability of the cluster centers and the promiscuity of the intra-riboswitch interactions were captured in interaction heat maps as shown in Supplementary Fig. S13. Unlike contact maps, interaction maps can discriminate between nucleotide proximity and actual base-pair interaction. As a result, interaction maps are useful for identifying conformational features widespread throughout most simulation clusters, such as the loss of Watson–Crick pairs G11–C31 and A10–U32, as well as an incremental increase in π-stacking found predominantly in the region between nucleotides 28 and 32 in the apo trajectory. The simulation and subsequent analysis of the predominant interactions suggest that the loss of Watson–Crick pairs in the bound structure might be compensated for by an increase in non-canonical base-pairing interactions in the apo structure (see Supplementary data for more details).

The X-ray crystal structure of the ligand-bound $preQ_1$ aptamer and our predicted apo model are shown in Fig. 1b, based on the structural features which are consistent throughout most clusters. Areas of major conformational change are located within the L1, L2, and S2 regions lining the ligand-binding pocket. Conversely, regions S1 and L3 remained unchanged by ligand removal in the simulation. It is noteworthy that when the ligand-binding pocket collapsed in the apo simulation, neighboring bases – C15 in particular – π-stacked and inserted into the pocket.

3.2. Experimental validation of $preQ_1$ aptamer dynamics with 2-AP reporters

Based on the conformational change predicted by our simulations, nucleotides at strategic locations in the riboswitch aptamer were substituted with 2-AP ribonucleobases in order to detect local conformational changes by monitoring 2-AP fluorescence after ligand addition [18]. Three aptamer constructs were prepared, and in each construct, a single nucleotide was selected (G4, G11, C15) which, upon binding of the ligand $preQ_1$, should (i) not change its environment (2AP4), (ii) become buried (2AP11), or (iii) become exposed (2AP15). Based on our computational predictions and the known environmental sensitivity of 2-AP emission, the fluorescence of the 2AP4, 2AP11, and 2AP15 constructs should remain unchanged, decrease, and increase upon ligand $preQ_1$ addition, respectively. Fig. 4 shows that the fluorescence intensities of the three 2-AP constructs in the apo state (red traces) are distinct. The initial fluorescence of 2AP4 was low (20 AU) relative to 2AP11 (80 AU) and 2AP15 (40 AU); apparent equilibrium dissociation constant (K_D) values were estimated from the fluorescence of each 2-AP reporter as a function of ligand concentration and found to be approximately 7.0 μM for 2AP4, 3.6 μM for 2AP11, and 1.5 μM for 2AP15.

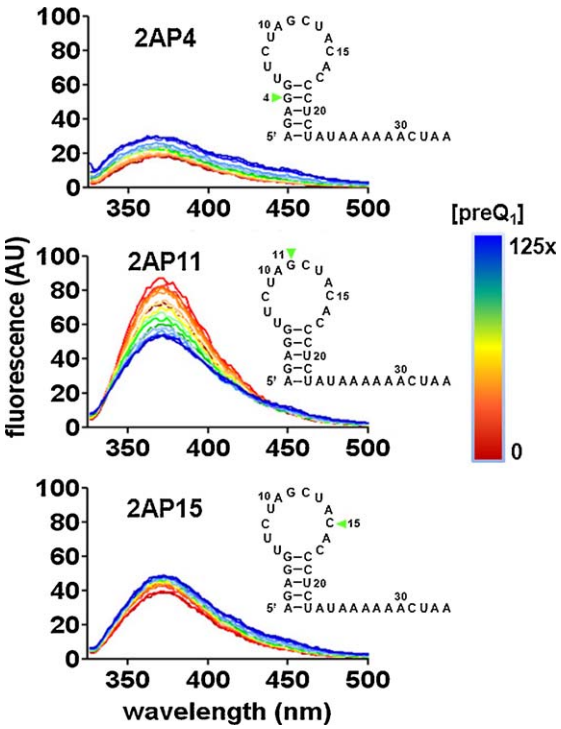

Fig. 4. Fluorescence spectra of 2-AP-substituted constructs before and after $preQ_1$ addition. The color scale indicates the relative concentration of ligand $preQ_1$ to RNA from 0 (red) to 125-fold (blue) molar excess; RNA concentration was 1 μM in 50 mM Tris–HCl, 20 mM $MgCl_2$, 100 mM KCl, pH 8.3, 25 °C. Green arrows indicate the 2-AP substituted nucleobase in the secondary structure diagram of each construct. (For interpretation of the references to color in this figure legend, the reader is referred to the web version of the article.)

Upon addition of $preQ_1$, a small increase in emission was observed for construct 2AP4. This is consistent with our model in which G4 is buried in the apo and bound states and involved in Watson–Crick pairing. The fluorescence signal for the apo form of 2AP15 was higher than for 2AP4, suggesting that C15 is less buried or engaged in a less restrictive interaction (e.g., π-stacking) than G4 in the absence of ligand, as seen in our model. Upon addition of $preQ_1$, 2AP15 also displayed a small increase in fluorescence emission. Nucleobase C15 is described as "extruded into solvent" in the crystal structure [17]; however, the orientation of this base varies throughout the different chains in the crystal, and in chain B, some atoms are missing. In addition, the NMR structure shows C15 flipped out in a different orientation (see Supplementary data for more modeling details). This suggests that the local environment surrounding position 15 is heterogeneous and could explain the fact that, in our experiments, 2AP15 is not as fluorescent in the bound state as we would expect from a completely solvent-extruded nucleotide.

In our simulations, the most striking conformational change observed in response to the absence of the $preQ_1$ ligand occurred

at position G11, for which the change in SASA from the bound to the unbound state was estimated to be approximately 32% (Fig. 2). In strong agreement with this prediction, 2AP11 also exhibited the largest fluorescence signal for the apo state (red trace), indicative of a more highly exposed nucleobase at position 11. Moreover, the fluorescence of this construct decreased substantially (50% reduction in intensity) when $preQ_1$ ligand was added, which is consistent with our simulated model. The hypothesis that follows from this result is that the presence of ligand $preQ_1$ induces a change in region S2 by providing interactions necessary to stabilize Watson–Crick pair G11–C31. Previous studies [5,35] suggest that the apo state of some riboswitches could be comprised of an ensemble of conformations. In light of the significant fluorescence change that we observe for the 2AP11 construct, we infer that this conformational change is likely shared by a large subpopulation of the ensemble.

In-line probing experiments [14] were performed to visualize global conformational changes in the riboswitch aptamer upon $preQ_1$ binding and to confirm that the 2-AP substituted constructs still retained characteristic structural features of the $preQ_1$ aptamer. The K_D value estimated from in-line probing data for the wild-type $preQ_1$ riboswitch aptamer (~45 nM) is consistent with the value of 50 nM reported by Roth et al. [14]. However, it is notable that all of our 2-AP-substituted constructs displayed reduced $preQ_1$ binding affinity in both in-line probing and 2-AP fluorescence experiments. $preQ_1$ binding was most severely reduced by 2AP substitution at position G4 ($K_D \sim 10\,\mu M$), despite the fact that 2-AP is reported to be a sufficient substitute for guanine in nucleic acid base pairing [36]. This experiment was repeated with a control construct bearing a 2-AP substitution for adenine at the adjacent position A3 (2AP3) (Supplementary Fig. S4); similar results for this 2AP3 construct as for 2AP4 indicate that the aptamer stem region itself is highly sensitive to mutations, even if they are as presumably minimal as aminopurine substitutions for purines. Nevertheless, constructs 2AP3 and 2AP4 were the most strongly quenched in the ligand-free state, and their fluorescence did not change substantially upon $preQ_1$ addition, as compared to the response exhibited by construct 2AP11. The G11 substitution appears to be less disruptive to ligand binding ($K_D \sim 5.1\,\mu M$), as was also the case for the C15 substitution ($K_D \sim 520$ nM). The latter observation is likely due to the fact that C15 does not appear to be engaged in Watson–Crick pairing in either the bound or apo conformations. These in-line probing experiments represent an important orthogonal control that allows us to confirm the retention of characteristic global conformational changes upon ligand addition even in the presence of 2-AP substitutions.

4. Conclusions

Based on our simulations and subsequent experimental validation, we propose that the apo form of the *Bacillus subtilis* $preQ_1$ riboswitch aptamer is structured and could also exhibit a pseudoknot form as shown in our simulated apo model. Interestingly, the simulated model does not show evidence of an exposed binding pocket. Instead, the pocket region in the bound structure collapses in the apo form due to the intrusion of nucleotides from loop L2. Upon ligand binding, the S2 loop undergoes a dramatic conformational change as G11–C31 come together into a Watson–Crick base pair, inducing the formation of the ligand-binding pocket. With these detailed snapshots of ligand-driven conformational changes, our results provide new insights into riboswitch ligand-binding mechanisms and illustrate the value of combining computer simulations with biophysical experiments to elucidate atomic-scale properties of riboswitches. While these ligand-driven conformational changes are critical to the function of riboswitches, further studies are warranted to address the equally significant role of kinetics in the function of the $preQ_1$ riboswitch aptamer [19,37,38]. Further in vivo experiments will be essential in determining whether the $preQ_1$ ligand triggers the aptamer as a ribo*switch* or irreversibly as a ribo*fuse* on physiologically relevant timescales.

Conflict of interest statement

None declared.

Funding

Novartis Institutes for BioMedical Research, Inc.

Acknowledgements

The authors thank the NIBR Education Office, NIBR RNAi Therapeutics, CADD, and NITAS groups, David Morrissey, Greg Paris, Jennifer Leeds, Michael Rebhan, Jose Duca, and Angel Garcia for their support.

Appendix A. Supplementary data

Supplementary data associated with this article can be found, in the online version, at doi:10.1016/j.jmgm.2011.07.006.

References

[1] A. Roth, R.R. Breaker, The structural and functional diversity of metabolite-binding riboswitches, Annu. Rev. Biochem. 78 (2009) 305–334.
[2] J.E. Barrick, K.A. Corbino, W.C. Winkler, A. Nahvi, M. Mandal, J. Collins, M. Lee, A. Roth, N. Sudarsan, I. Jona, J.K. Wickiser, R.R. Breaker, New RNA motifs suggest an expanded scope for riboswitches in bacterial genetic control, Proc. Natl. Acad. Sci. U.S.A. 101 (2004) 6421–6426.
[3] M. Sharma, G. Bulusu, A. Mitra, MD simulations of ligand-bound and ligand-free aptamer: molecular level insights into the binding and switching mechanism of the add A-riboswitch, RNA 15 (2009) 1673–1692.
[4] A. Villa, J. Wohnert, G. Stock, Molecular dynamics simulation study of the binding of purine bases to the aptamer domain of the guanine sensing riboswitch, Nucleic Acids Res. 37 (2009) 4774–4786.
[5] C. Stoddard, R. Montange, S. Hennelly, R. Rambo, K. Sanbonmatsu, R. Batey, Free state conformational sampling of the SAM-I riboswitch aptamer domain, Structure 18 (2010) 787–797.
[6] D. Wunnicke, D. Strohbach, J.E. Weigand, B. Appel, E. Feresin, B. Suess, S. Müller, H.-J. Steinhoff, Ligand-induced conformational capture of a synthetic tetracycline riboswitch revealed by pulse EPR, RNA 17 (2010) 182–188.
[7] R.C. Wilson, A.M. Smith, R.T. Fuchs, I.R. Kleckner, T.M. Henkin, M.P. Foster, Tuning riboswitch regulation through conformational selection, J. Mol. Biol. 405 (2011) 926–938.
[8] A.D. Garst, A. Heroux, R.P. Rambo, R.T. Batey, Crystal structure of the lysine riboswitch regulatory mRNA element, J. Biol. Chem. 283 (2008) 22347–22351.
[9] A. Serganov, L. Huang, D.J. Patel, Structural insights into amino acid binding and gene control by a lysine riboswitch, Nature 455 (2008) 1263–1267.
[10] O.M. Ottink, S.M. Rampersad, M. Tessari, G.J.R. Zaman, H.A. Heus, S.S. Wijmenga, Ligand-induced folding of the guanine-sensing riboswitch is controlled by a combined predetermined-induced fit mechanism, RNA 13 (2007) 2202–2212.
[11] U.D. Priyakumar, A.D. MacKerell Jr., Role of the adenine ligand on the stabilization of the secondary and tertiary interactions in the adenine riboswitch, J. Mol. Biol. 396 (2010) 1422–1438.
[12] M. Kang, R. Peterson, J. Feigon, Structural insights into riboswitch control of the biosynthesis of queuosine, a modified nucleotide found in the anticodon of tRNA, Mol. Cell 33 (2009) 784–790.
[13] Q. Zhang, M. Kang, R.D. Peterson, J. Feigon, Comparison of solution and crystal structures of $preQ_1$ riboswitch reveals calcium-induced changes in conformation and dynamics, J. Am. Chem. Soc. 133 (2011) 5190–5193.
[14] A. Roth, W.C. Winkler, E.E. Regulski, B.W.K. Lee, J. Lim, I. Jona, J.E. Barrick, A. Ritwik, J.N. Kim, R. Welz, D. Iwata-Reuyl, R.R. Breaker, A riboswitch selective for the queuosine precursor $preQ_1$ contains an unusually small aptamer domain, Nat. Struct. Mol. Biol. 14 (2007) 308–317.

[15] J.S. Reader, D. Metzgar, P. Schimmel, V. de Crécy-Lagard, Identification of four genes necessary for biosynthesis of the modified nucleoside queuosine, J. Biol. Chem. 279 (2004) 6280–6285.
[16] D. Iwata-Reuyl, Biosynthesis of the 7-deazaguanosine hypermodified nucleosides of transfer RNA, Bioorg. Chem. 31 (2003) 24–43.
[17] D.J. Klein, T.E. Edwards, A. Ferré-D'Amaré, Cocrystal structure of a class I $preQ_1$ riboswitch reveals a pseudoknot recognizing an essential hypermodified nucleobase, Nat. Struct. Mol. Biol. 16 (2003) 343–344.
[18] U. Rieder, K. Lang, C. Kreutz, N. Polacek, R. Micura, Evidence for pseudoknot formation of class I $preQ_1$ riboswitch aptamers, Chembiochem 10 (2009) 1141–1144.
[19] U. Rieder, C. Kreutz, R. Micura, Folding of a transcriptionally acting $preQ_1$ riboswitch, Proc. Natl. Acad. Sci. U.S.A. 107 (2010) 10804–10809.
[20] R.C. Spitale, A.T. Torelli, J. Krucinska, V. Bandarian, J.E. Wedekind, The structural basis for recognition of the $preQ_0$ metabolite by an unusually small riboswitch aptamer domain, J. Biol. Chem. 284 (2008) 11012–11016.
[21] J. Feng, N.G. Walter, C.L. Brooks, Cooperative and directional folding of the $preQ_1$ riboswitch aptamer domain, J. Am. Chem. Soc. 133 (2011) 4196–4199.
[22] H. Akimoto, E. Imamiyz, T. Hitaka, H. Nomura, S. Nishimura, Synthesis of queuine, the base of naturally occurring hypermodified nucleoside (queuosine), and its analogues, J. Chem. Soc., Perkin Trans. 1 (1988) 1637–1644.
[23] E.E. Regulski, R.R. Breaker, In-line probing analysis of riboswitches, Methods Mol. Biol. (Clifton, NJ) 419 (2008) 53–67.
[24] W.L. Jorgensen, J. Chandrasekhar, J.D. Madura, R.W. Impey, M.L. Klein, Comparison of simple potential functions for simulating liquid water, J. Chem. Phys. 79 (1983) 926–935.
[25] J. Wang, R.M. Wolf, J.W. Caldwell, P.A. Kollman, D.A. Case, Development and testing of a general amber force field, J. Comput. Chem. 25 (2004) 1157–1174.
[26] E.J. Sorin, V.S. Pande, Exploring the helix-coil transition via all-atom equilibrium ensemble simulations, Biophys. J. 88 (2005) 2472–2493.
[27] P.M. Petrone, C.D. Snow, D. Lucent, V.S. Pande, Side-chain recognition and gating in the ribosome exit tunnel, Proc. Natl. Acad. Soc. U.S.A. 105 (2008) 16549–16554.
[28] B. Hess, C. Kutzner, D. van der Spoel, E. Lindahl, GROMACS 4: algorithms for highly efficient, load-balanced, and scalable molecular simulation, J. Chem. Theory Comput. 4 (2008) 435–447.
[29] D.V.D. Spoel, E. Lindahl, B. Hess, G. Groenhof, A.E. Mark, H.J.C. Berendsen, GROMACS: fast, flexible, and free, J. Comp. Chem. 26 (2005) 1701–1718.
[30] B. Hess, H. Bekker, H. Berendsen, J. Fraaije, LINCS: a linear constraint solver for molecular simulations, J. Comp. Chem. 18 (1997) 1463–1472.
[31] H.J.C. Berendsen, J.P.M. Postma, W.F. van Gunsteren, A. DiNola, J.R. Haak, Molecular dynamics with coupling to an external bath, J. Chem. Phys. 81 (1984) 3684–3690.
[32] J. Lipfert, A.Y.L. Sim, D. Herschlag, S. Doniach, Dissecting electrostatic screening, specific ion binding, and ligand binding in an energetic model for glycine riboswitch folding, RNA 16 (2010) 708–719.
[33] J.D. Ballin, S. Bharill, E.J. Fialcowitz-White, I. Gryczynski, Z. Gryczynski, G.M. Wilson, Site-specific variations in RNA folding thermodynamics visualized by 2-aminopurine fluorescence, Biochemistry 46 (2007) 13948–13960.
[34] R.D. Gray, L. Pettracone, R. Buscaglia, J.B. Chaires, 2-Aminopurine as a probe for quadruplex loop structures, Methods Mol. Biol. (Clifton NJ) 608 (2010) 121–136.
[35] M. Ali, J. Lipfert, S. Seifert, D. Herschlag, S. Doniach, The ligand-free state of the TPP riboswitch: a partially folded RNA structure, J. Mol. Biol. 396 (2010) 153–165.
[36] A. Sielaff, H. Mackay, T. Brown, M. Lee, 2-Aminopurine/cytosine base pair containing oligonucleotides: fluorescence spectroscopy studies on DNA–polyamide binding, Biochem. Biophys. Res. Commun. 369 (2008) 630–634.
[37] J.K. Wickiser, M.T. Cheah, R.R. Breaker, D.M. Crothers, The kinetics of ligand binding by an adenine-sensing riboswitch, Biochemistry 44 (2005) 13404–13414.
[38] J.K. Wickiser, Kinetics of riboswitch regulation studied by in vitro transcription, Methods Mol. Biol. (Clifton NJ) 540 (2009) 53–63.